Subsurface crack initiation and propagation mechanisms in gigacycle fatigue

Zhiyong Huang, Danièle Wagner, Claude Bathias, Paul C. Paris

Subsurface crack initiation and propagation mechanisms in gigacycle fatigue

Zhiyong Huang [a,b], Danièle Wagner [a,*], Claude Bathias [a], Paul C. Paris [c]

[a] Université Paris Ouest Nanterre La Défense, 50 Rue de Sèvres, 92410 Ville d'Avray, France
[b] Nanjing University of Aeronautics and Astronautics, 29 Yu Dao Street, 210016 Nanjing, China
[c] LAMEFIP EA 2727, Arts et Métiers, Esplanade des Arts et Métiers, 33405 Talence Cedex, France

Abstract

In the very high cycle regime ($N_f > 10^7$ cycles) cracks can nucleate on inclusions, "supergrains" and pores, which leads to fish-eye propagation around the defect. The initiation from an inclusion or other defect is almost equal to the total crack growth lifetime, perhaps much more than 99% of this lifetime in many cases. Integration of the Paris law allows one to predict the number of cycles to crack initiation. A cyclic plastic zone around the crack exists, and recording the surface temperature of the sample during the test may allow one to follow crack propagation and determine the number of cycles to crack initiation. A thermo-mechanical model has been developed. In this study several fish-eyes from various materials have been observed by scanning electron microscopy, and the fractographic results analyzed as they related to the mechanical and thermo-mechanical models.

Keywords: Very high cycle fatigue; Metals and alloys; Scanning electron microscopy; Subsurface crack initiation

1. Introduction

In fatigue tests, depending on the strain or stress level, three domains exist: the low cycle fatigue domain ($N_f < 10^4$ cycles, "oligocycle" domain), the high cycle fatigue domain ($10^4 < N_f < 10^7$ cycles, megacycle domain) and the very high cycle fatigue domain ($N_f > 10^7$ cycles, gigacycle domain). The latter is now under investigation [1] with the development of devices (piezoelectric fatigue machines) working at high frequency (20 or 30 kHz), allowing one to obtain 10^8 or more cycles in a reasonable time. These tests have shown that fracture can occur at 10^9 or more cycles, which is problematic, since many components and structures for numerous applications require a fatigue life greater than 10^8 cycles.

According to the fatigue domain, different types of crack initiation occur. In the gigacycle fatigue domain the initiation site may be located in an internal zone or at the surface. When the crack initiation site is in the interior, this leads to the formation of a "fish-eye" on the fracture surface, with the origin of the fatigue crack being an inclusion, a "supergrain" (microstructural inhomogeneity) or porosity. On the macroscopic scale, under an optical microscope (or to the naked eye), the fish-eye area looks white, whereas the region outside the fish-eye looks grey. In almost all cases this fish-eye appears circular, with a dark area in the center, inside which the crack initiation site is located. Controversy exists as to the origin of this dark area, which has been termed the "optically dark area" (ODA) by Murakami [2], the "fine granular area" (FGA) by Sakai [3] and "granular bright facet" (GBF) by Shiozawa [4]. According to Murakami et al., the mechanism of formation of ODAs is presumed to be microscale fatigue fracture caused by cyclic stress coupled with internal hydrogen trapped within non-metallic inclusions. It is presumed that when the size of

* Corresponding author. Tel.: +33 0 1 40 97 57 76; fax: +33 0 1 40 97 48 10.
E-mail address: daniele.wagner@u-paris10.fr (D. Wagner).

an ODA exceeds the intrinsic material fatigue limit critical size in the absence of hydrogen the crack grows without the assistance of hydrogen, and the crack cannot become non-propagating. According to Sakai et al., the mechanism of formation of FGAs is by intensive polygonisation induced around the inclusion, followed by micro-debonding, which can coalesce, leading to a FGA. According to Shiozawa et al., the mechanism of formation of GBFs is the separation of boundaries between carbides particles and the matrix. At the microscopic level, Mugrahbi [5] showed that the initiation of a fatigue crack in the gigacycle fatigue regime can be described in terms of the microstructurally irreversible portion of the cumulative cycle strain.

As ODA, FGA and GBF are formed around inclusions, related to persistent slip band formation, all authors agree that crack growth (stages I and II) is governed by the Paris law.

Several models have been used to predict the number of cycles to initiate a fatigue crack from an inclusion, more or less successfully [1]. In the gigacycle fatigue range the integration of the Paris law [6,7] allows one to predict the number of cycles for fish-eye growth and to obtain the number of cycles at crack initiation by subtraction. The number of cycles for crack propagation in the fish-eye calculated by the model is very small compared with the total fatigue life.

For internal initiation it is difficult to determine the number of cycles to initiation. Using a thermo-mechanical approach, Wagner et al. [8–10] determined the number of cycles to initiation (including for internal initiation) by recording the surface temperature of the sample during the test, which allows one to follow crack propagation and determine the number of cycles for crack initiation. These results confirm that in the gigacycle domain more than 90% of the total lifetime involves initiation of the crack.

The purpose of this study was to complement the mechanical and thermo-mechanical approach by fractographic observations when a crack initiates at an internal defect and forms a fish-eye on the fracture surface. These observations were conducted on two steels (quenched and tempered low-alloyed chromium steel and a normalized C–Mn steel) and on an Al–Si–Cu alloy.

2. Mechanical approach

The model of Paris et al. [6,7] for crack growth in a fish-eye is based on integration of the Paris–Hertzberg law, as in Figs. 1 and 2. Reviews on crack growth and thresholds allow to estimate the slope change at $da/dN = \mathbf{b}$ and $\Delta K_{\text{eff}}/E\sqrt{\mathbf{b}} = 1$, where $\mathbf{b}$ is the Burgers' vector and E is the elastic modulus.

At the beginning of crack growth a small crack a_0 (with no crack closure and corresponding to $\Delta K_{\text{eff}}/E\sqrt{\mathbf{b}} = 1$) starts from a defect of size a_{int}. This short crack becomes a long crack at a_{i}. The growth rate is greater for small cracks than for long cracks. The transition point from a short crack to a long crack is located at a point x in terms

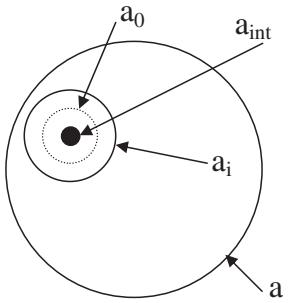

Fig. 1. Modelling of relevant crack sizes in the mechanical model [6,7].

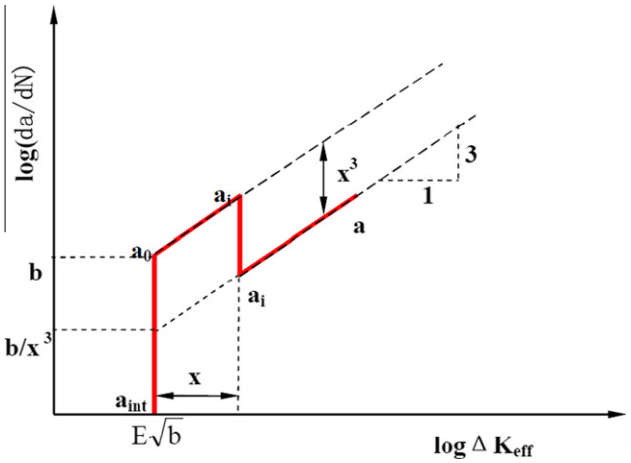

Fig. 2. Modelling of crack growth in the fish-eye [6,7].

of the stress intensity factor from the threshold for short cracks (Fig. 2). The factor x has been observed at a maximum of around three for low load ratios ($R = 0$).

The total crack growth lifetime for an internal failure can be estimated by addition of the following lifetimes: $N_{\text{aint}\rightarrow a_0}$, below threshold from an initial crack size a_{int} to a_0; $N_{a_0\rightarrow a_i}$, small crack from an initial crack size a_0 to a_{i}; $N_{a_i\rightarrow a}$, large crack from transition small to large crack point a_{i} to a (final crack).

3. Thermo-mechanical approach

Previous studies [8–10] have investigated the temperature evolution on the surface specimens during tests in the gigacycle fatigue domain. Two recordings are given Figs. 3 and 4 for a low-alloyed chromium steel. Fig. 3 is the entire recording from the beginning of the test. Initially the temperature increased rapidly, followed by a stable regime. The temperature variation depended on the material, microstructure and on the stress amplitude level ($\Delta\sigma$); the higher the stress, the higher the temperature reached. At the end of the test (before final fracture) the temperature increased rapidly, corresponding to crack propagation from a defect. Fig. 4 is an enlargement (taken from another specimen of low-alloyed chromium steel) of the end of the test. In Fig. 3 the sample was cooled during the test, whereas it was not in the case of the test in Fig. 4.

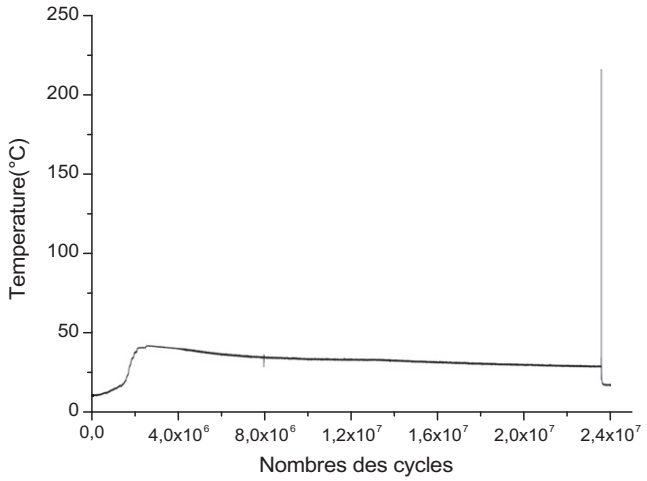

Fig. 3. Temperature evolution on the sample surface during a gigacycle fatigue test.

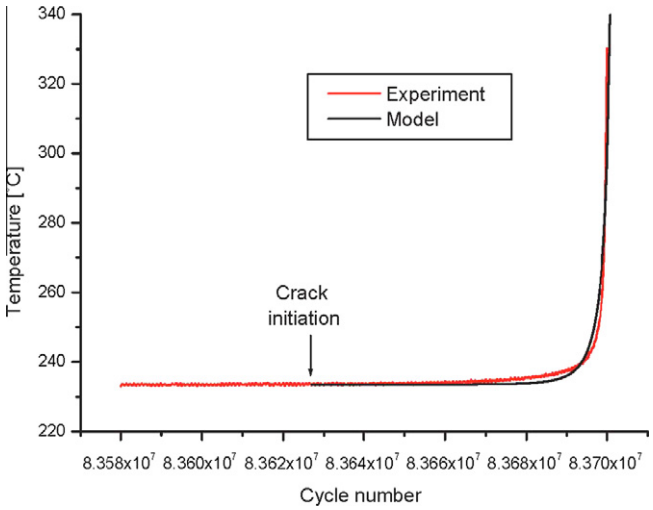

Fig. 4. Temperature evolution at the end of the test (from the model and experiment).

In order to better understand these thermal effects and to make a connection between crack initiation and propagation, a thermo-mechanical model was developed [8]. Numerical solution of the thermal problem allows determination of temperature field evolution with time in the specimen. A comparison between the test and model shows a good correlation (Fig. 4). This shows that the rapid increase in temperature at the end of the test corresponded to fish-eye initiation and the number of cycles at initiation could be accurately determined.

4. Fractographic approach

Firstly, on the macroscopic scale the appearance of a fish-eye is not the same by optical microscopy (OM) and scanning electron microscopy (SEM). Figs. 5 and 6 show observations of the same sample by OM and SEM. These results were obtained on carburized low-alloy chromium

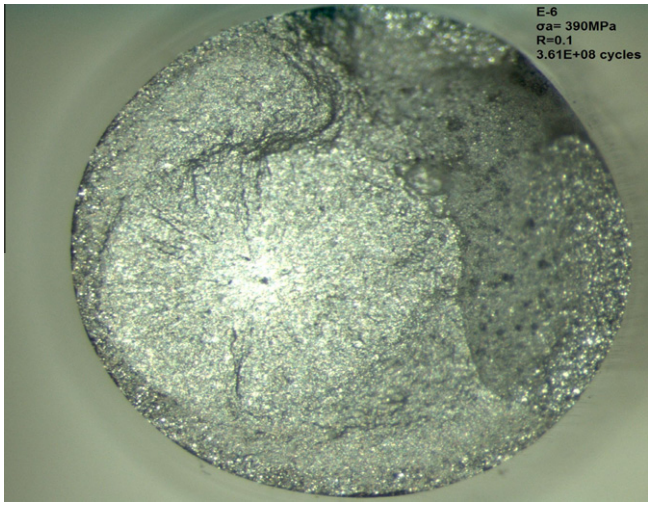

Fig. 5. Observation of the fracture surface by optical microscopy (bearing steel, specimen E6).

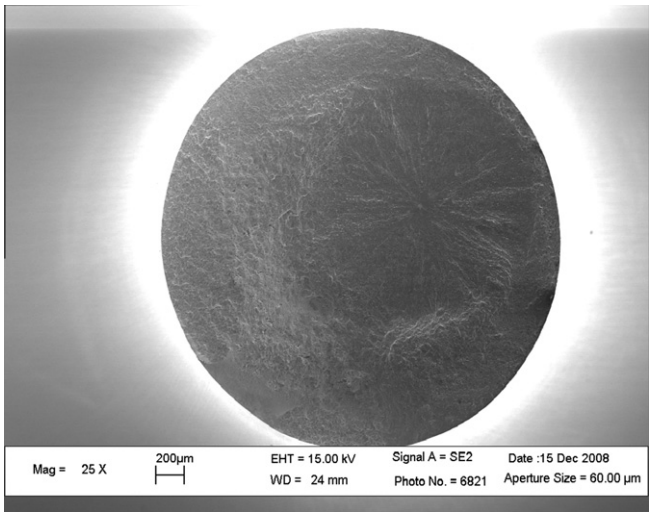

Fig. 6. Observation of the fracture surface by SEM (bearing steel, specimen E6).

steel. The microstructure was martensite with retained austenite. In the optical micrograph the crack initiation site appears as a dark point (a well-named ODA), whereas in the SEM image its appearance is not so clear as at low magnification. A white zone is present in the optical micrograph surrounding the dark point. In the SEM observation this zone is rather flat (Fig. 7) and circular (penny-shaped). Outside this white zone one can see a wide fracture surface having a large radial ridge pattern in both the OM and SEM micrographs.

4.1. Dark area observations

The dark area zone corresponds to the crack initiation zone, which, in the gigacycle fatigue domain, can be an inclusion, a metallurgical heterogeneity (“supergrain”) or a pore (for cast products). As reported by Murakami et al. [2–4], at high magnification (Figs. 7–10) the dark area

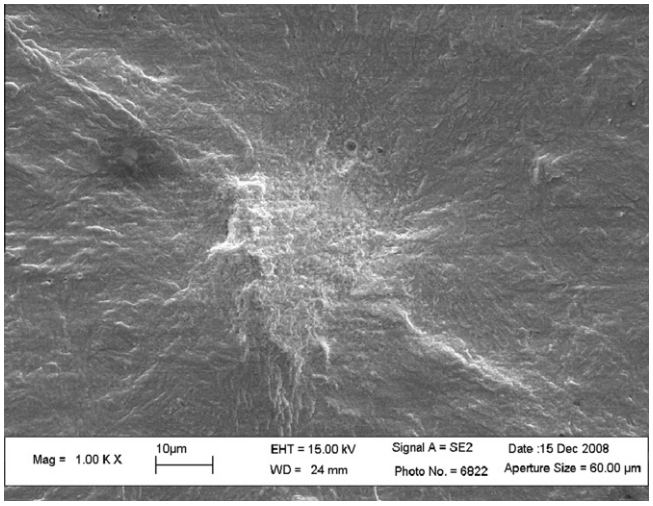

Fig. 7. Crack initiation site (a supergrain in an ODA/FGA) observed by SEM for specimen E6.

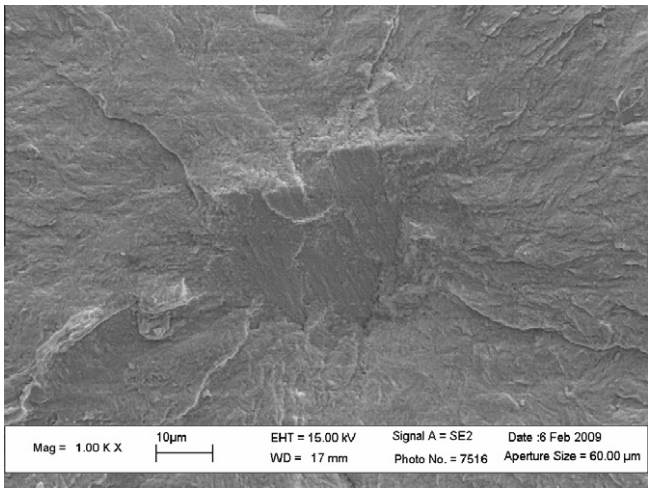

Fig. 8. Crack initiation site (a supergrain in an ODA/FGA) observed by SEM (bearing steel, specimen C24).

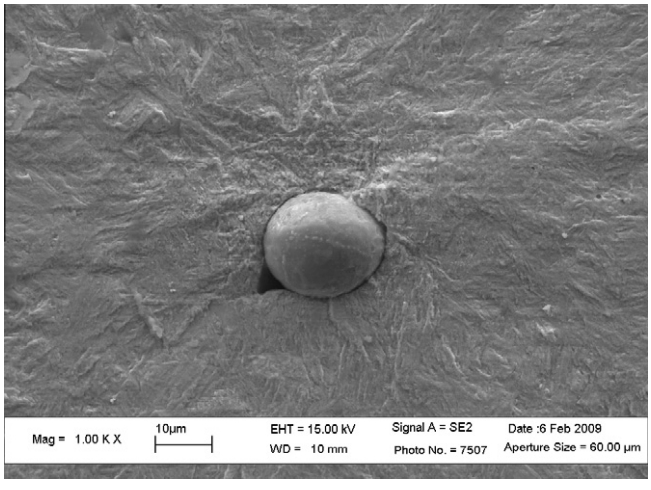

Fig. 9. Crack initiation site (an inclusion in an ODA/FGA) observed by SEM (bearing steel, specimen E13).

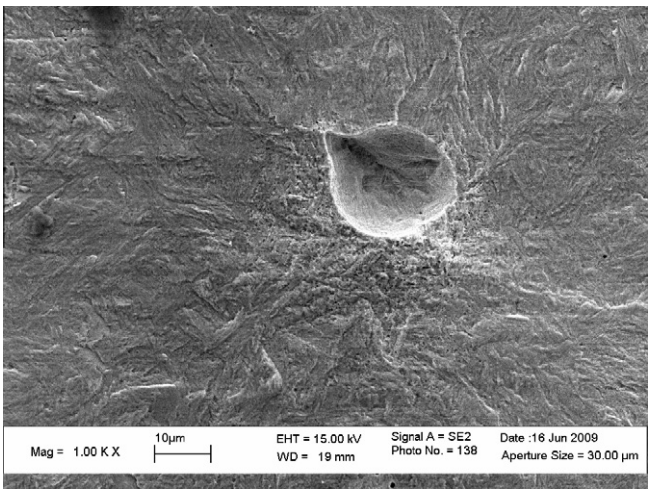

Fig. 10. Crack initiation site (an inclusion in an ODA/FGA) observed by SEM (bearing steel, specimen E13, on the other side of the fracture surface).

appears as a granular layer (the well-named FGA or GBA), as seen in the SEM. The explanation of the formation of this FGA differs among researchers, due to controversy as to the origin of this zone.

Fig. 7 (which corresponds to the crack initiation zone in Figs. 5 and 6) and Fig. 8 show crack initiation on a "supergrain" (probably a large soft retained austenite grain). In Fig. 7 the FGA has spread over and around the entire grain; in Fig. 8 the FGA is located above and below the "supergrain". Figs. 9 and 10 show the two sides of the fracture surface for a sample of the same material with crack initiation located at an inclusion (mixed inclusion of Al, Si, Ca, Mg, Mn and S). The FGA had spread from the sides of the inclusion and the trace of this FGA was the same on the two fracture surfaces.

4.2. "*Penny-shaped area*" *observations*

Whatever the crack initiation site (inclusion, "supergrain" or porosity), the fracture surface eventually became circular ("penny-shaped") around the initiation site. Figs. 11–17 show examples of such behaviour (as expected from the variation of the stress intensity factor around the periphery of the crack).

Fig. 11 shows the area around the ODA/FGA for the specimen in Fig. 7, obtained from low-alloyed chromium steel. This zone was flat. Martensitic platelet microstructure was visible. It is expected that in this zone there would be no crack closure. Figs. 13 and 14 correspond to the "penny-shaped" area of Figs. 8–10. The same conclusions can be drawn.

Fig. 15 (an optical microscope observation) and Fig. 16 (a SEM observation) show a fish-eye obtained in a ferrite–pearlite C–Mn steel with a high sulphur content (0.030%). The longitudinal axis of the test sample was perpendicular to the rolling direction (TL orientation). The origin of crack initiation was in manganese sulphide (MnS), which

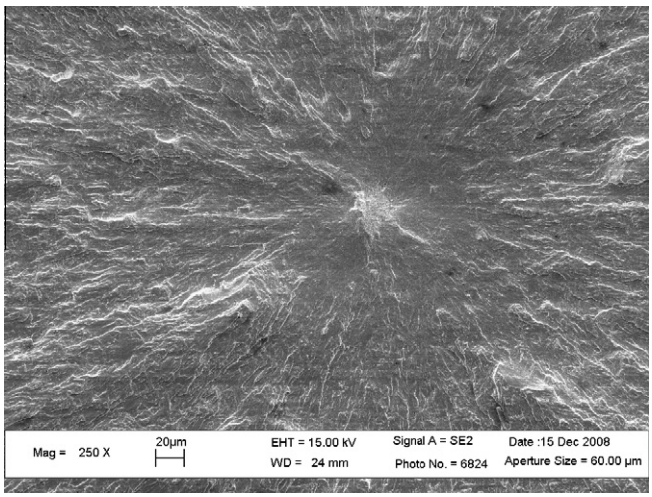

Fig. 11. "Penny-shaped area", corresponding to Fig. 7.

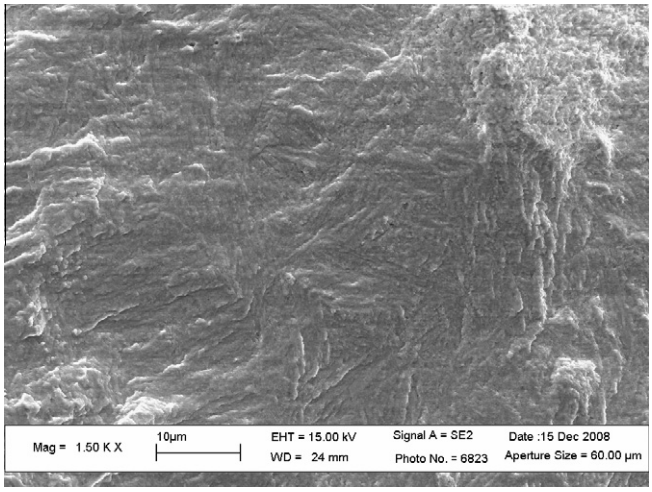

Fig. 12. Detail of the "penny-shaped area" of Fig 11.

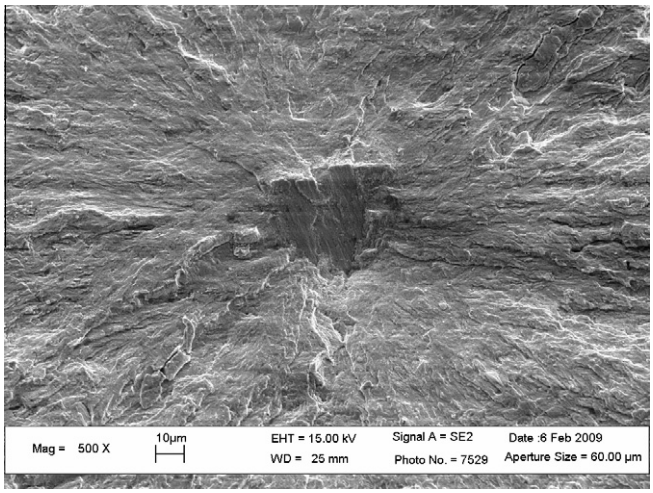

Fig. 13. "Penny-shaped area" observation, corresponding to Fig 8.

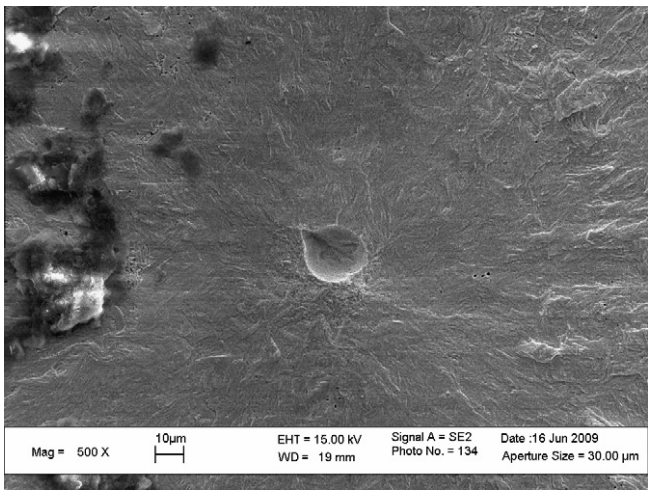

Fig. 14. "Penny-shaped area" observation, corresponding to Fig 10.

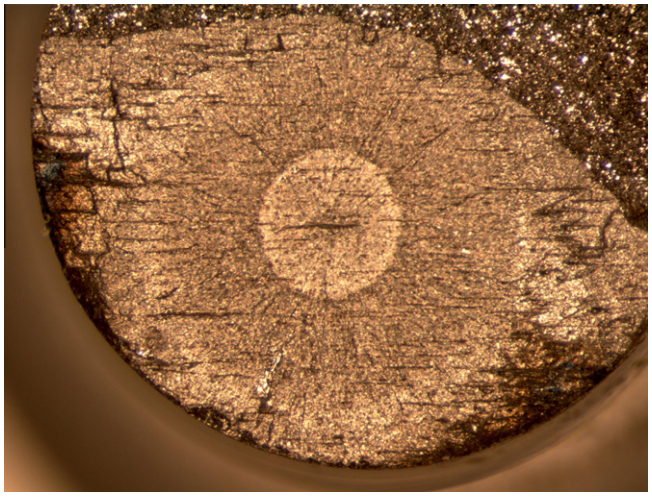

Fig. 15. Optical microscope observation in a C–Mn steel.

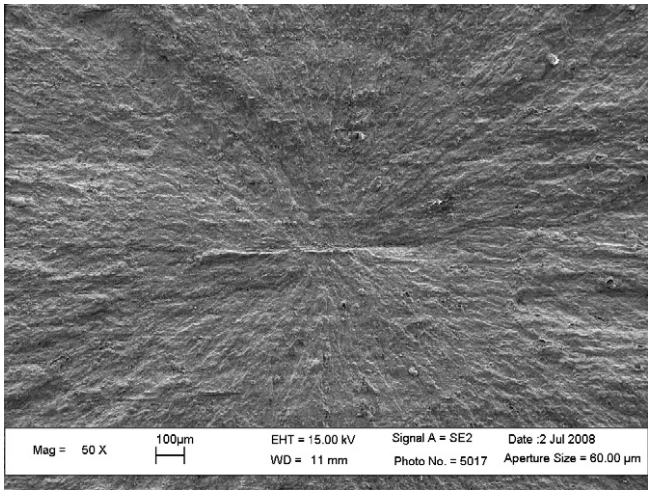

Fig. 16. SEM observation of a C–Mn steel.

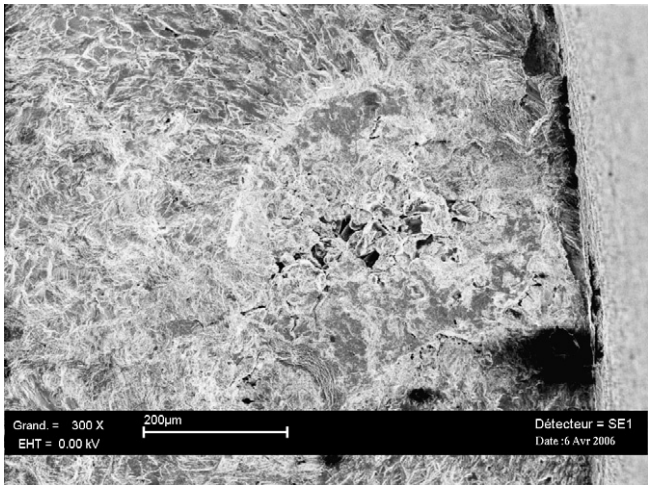

Fig. 17. SEM crack initiation site (porosity) in an Al–Si–Cu alloy.

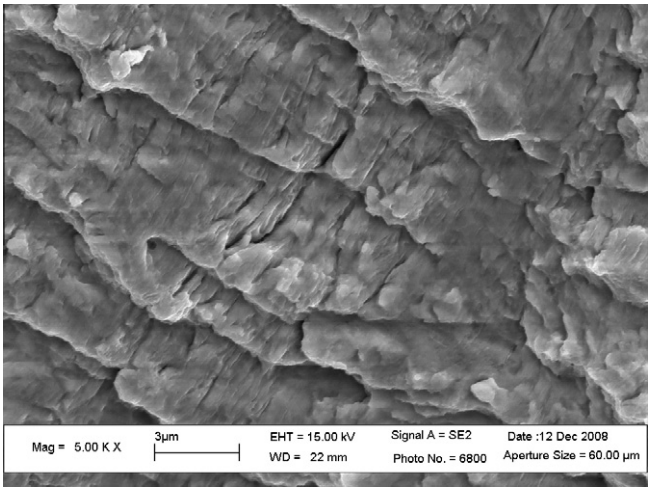

Fig. 18. Striations in the radial ridged zone (bearing steel).

failed in its longest direction. Even with an elongated inclusion the crack shape became circular after a short propagation, again in good agreement with linear-elastic fracture-mechanics predictions.

Fig. 17 is a fish-eye obtained in a cast Al–Si–Cu alloy. The origin of crack initiation was a pore. Again, the crack shape became semi-circular around the elongated porosity close to the surface.

At the end of this "penny-shaped" zone small concentric radial ridges appeared (Figs. 11–17), beyond which large radial ridges occurred.

4.3. Fracture surface with large radial ridges

In this fish-eye zone high magnification SEM observations show striations (Figs. 18–21). All the observations and measurements were made on several specimens of the low-alloyed chromium steel. Each picture at high magnification (×5000) was referenced to a picture at lower magnification (×100) to show the location of the striations with regard to the crack initiation site.

For each zone with striations the mean distance between striations was measured and the associated ΔK value ($\Delta K = 2\Delta\sigma/\pi\sqrt{\pi a}$) was calculated. Fig. 22 gives the evolution of the striation spacing log$e$ vs. log ΔK. The equation for the straight line is $\log e = 2\log(\Delta K) - 10.97$. The slope of the straight line was in good agreement with the crack tip opening displacement (CTOD) model, in which the striation spacing is a function of ΔK^2.

Until now [1], it has been reported that a vacuum is present inside the fish-eye. So it is surprising that well-defined striations are present in the large radial ridge zone. A review of the environment effect by Petit and Sarrazin-Baudoux [12] suggested that no striations appear in a vacuum. Nevertheless, striations in vacuum do appear possible, but are less clearly defined.

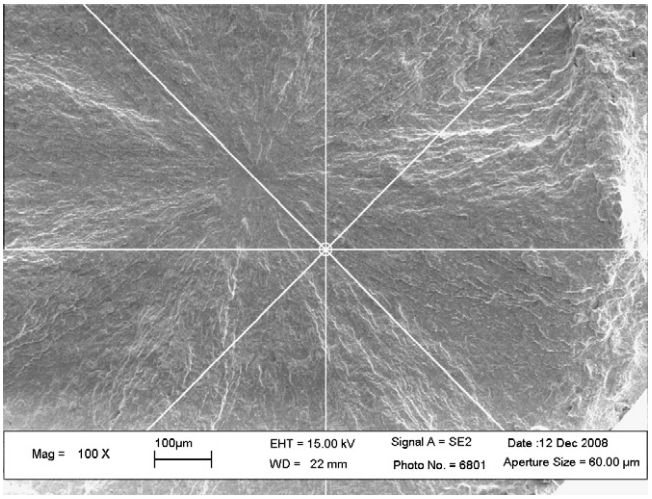

Fig. 19. Location at which the striations in Fig. 18 were measured.

In all probability the environment in the fish-eye is not a vacuum, because during steel fabrication a partial pressure of air results or, as suggested by Murakami [2] and Takai [11], if hydrogen is desorbed from non-metallic inclusions (at the initiation site or inclusions on the crack path during propagation), the environment is not a vacuum.

5. Identification of the models

Detailed fractographic observations of the fish-eye fracture surface showed several zones. The purpose of this section is to relate these fractographic observations to the mechanical model.

Table 1
Crack length values measured from fractographic observations and corresponding ΔK values (for specimen E13).

	$\Delta\sigma$ (MPa)	N_f	a (µm)	a_{i1} (µm)	a_0 (µm)	a_{int} (µm)	ΔK_{ai1} (MPa$\sqrt{m}$)	ΔK_{ai2} (MPa$\sqrt{m}$)	ΔK_{a_0} (MPa$\sqrt{m}$)
E13	800	5.25E + 07	550	62.5	17.19	10.03	7.2	7.8	3.8

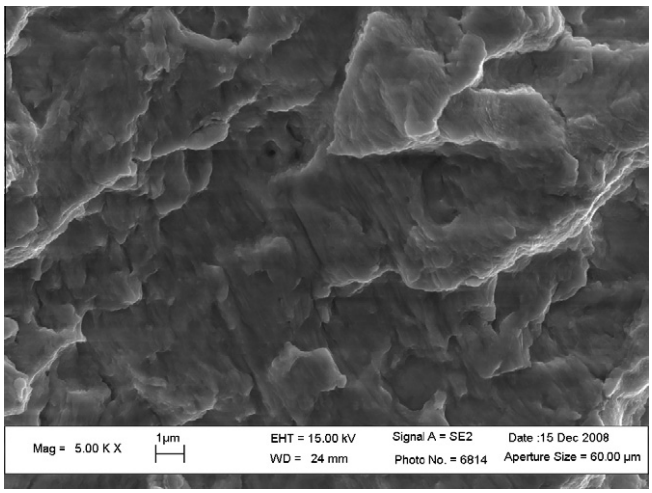

Fig. 20. Striations in the radial ridged zone (bearing steel).

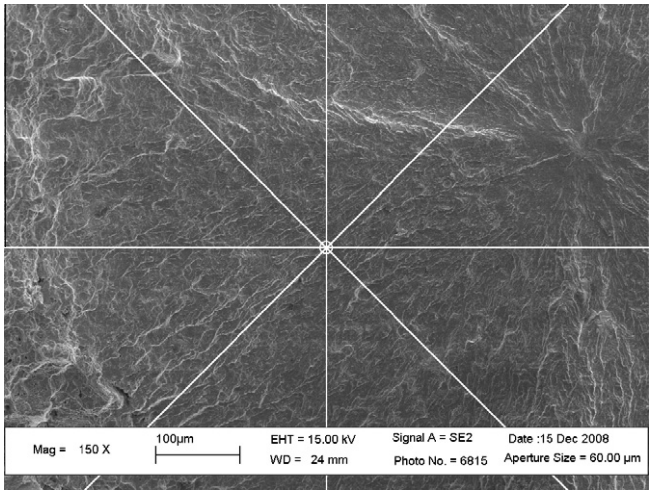

Fig. 21. Location at which the striations in Fig. 20 were measured.

The later (and largest) zone of the fish-eye, from a_i to a in the mechanical model, corresponds to the large radial ridge zone (Fig. 23). For crack length a the fracture toughness of the material is reached and rapid and final fracture occurs. In this zone (from a_i to a) striations are visible and propagation is large crack growth in stage II.

In the mechanical model the transition short crack to long crack is steep at a crack length equal to a_i (Fig. 2). For the fractographic observations, the "penny-shaped zone", in which martensitic platelet microstructure is seen (for the low-alloyed steel) is related to short crack propagation, where no crack closure is present. The crack length of the "penny-shaped zone" is termed a_{i-1}. Between the "penny-shaped zone" and the large radial ridge zone, a zone with small radial ridges is observed. At the end of this zone, termed a_{i-2}, striations are sometimes visible. So, as expected, the transition short crack to long crack is not steep, but localized around a_i between a_{i-1} and a_{i-2} (as shown for one specimen in Fig. 24).

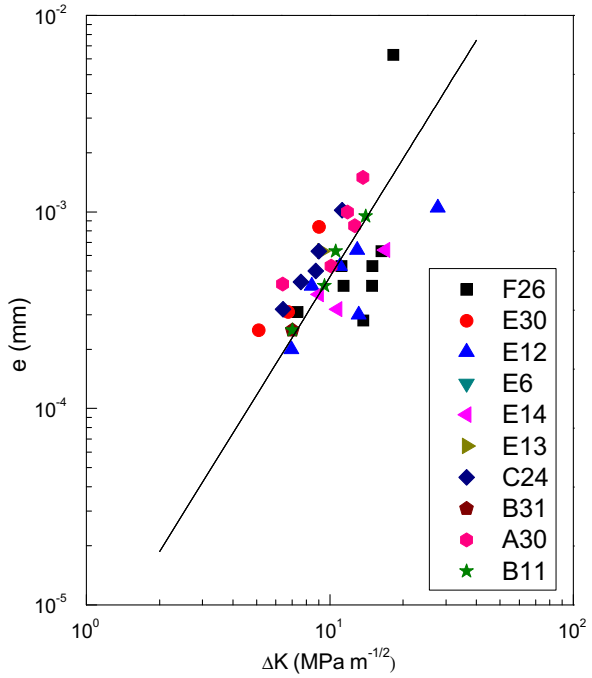

Fig. 22. Striation spacing e vs. ΔK (bearing steel).

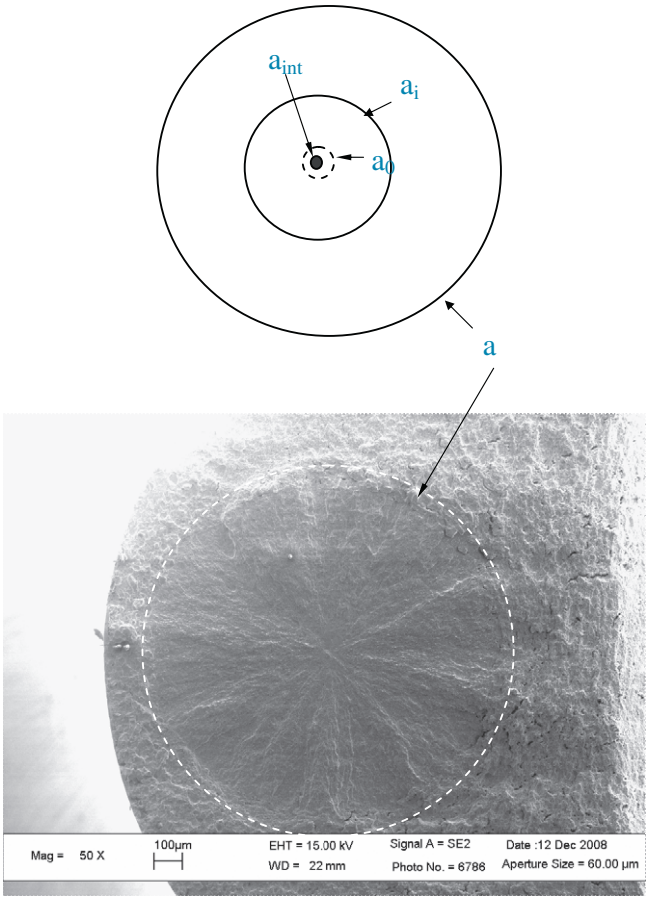

Fig. 23. Identification of the final crack length (bearing steel).

In the mechanical model the threshold is taken as $da/dN = \mathbf{b}$ and $\Delta K_{eff}/E\sqrt{\mathbf{b}} = 1$ and corresponds to a crack

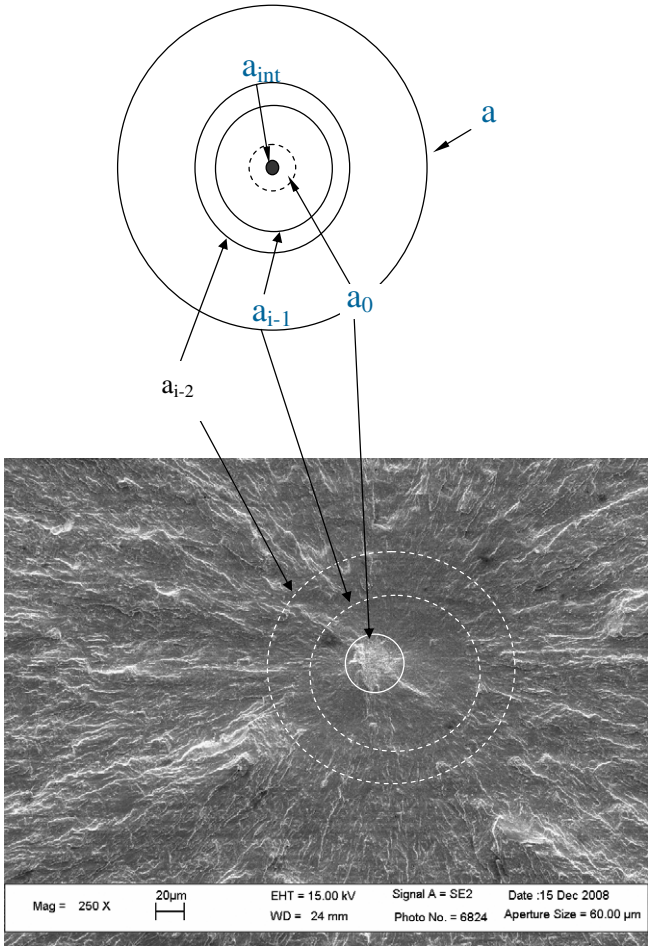

Fig. 24. Identification of the relevant crack sizes in the mechanical model (bearing steel).

length initiation a_0. In the SEM observations a FGA is observed (probably the dark area in the optical observations) around the defect, from which crack initiation occurs. This zone (Fig. 24) from a_{int} (defect size) to a_0 (FGA zone) is due to the formation of an irreversible persistent slip band in grains well oriented around the defect (Figs. 7–10).

Quantitative measurements of the different zones were performed (on the low-alloy steel tested at $R = 0.1$) whenever possible. The final crack length a of the fish-eye was not considered, because the specimens studied had a carburized surface which induced a hard layer on the surface specimen, disturbing the true final crack length. For the other characteristic lengths the following results were obtained: $40\ \mu\text{m} < a_{i-2} < 140\ \mu\text{m}$; $30\ \mu\text{m} < a_{i-1} < 70\ \mu\text{m}$; $15\ \mu\text{m} < a_0 < 25\ \mu\text{m}$; $7\ \mu\text{m} < a_{\text{int}} < 19\ \mu\text{m}$. a_{int}, defect radius leading to initiation; a_0, fine granular zone radius due to the formation of irreversible persistent slip bands; a_{i-1}, penny-shaped zone crack radius; a_{i-2}, end of the transition small crack to large crack; a, fish-eye final radius.

The radius a_0 (FGA) is the most difficult to measure. The uncertainty is about ±15% of the measured values. For the radii a_{i-1} and a_{i-2} the scattering is lower (±10%).

For each crack measurement ΔK values ($\Delta K = 2\Delta\sigma/\pi\sqrt{\pi a}$) were calculated. The results are reported in Fig. 25 vs. the number of cycles at failure. Whatever the number of cycles at failure, ΔK_{aint}, ΔK_{a_0}, $\Delta K_{a_{i-1}}$ and $\Delta K_{a_{i-2}}$ remained constant or decreased slightly, which was expected for the same material.

In the mechanical model the threshold was predicted at $da/dN = \mathbf{b}$ and $\Delta K_{\text{eff}}/E\sqrt{\mathbf{b}} = 1$. This corresponds to the length a_0. Taking $E = 210{,}000$ MPa (for steels) and $\mathbf{b} = 0.3$ nm, the value of ΔK_{eff} is 3.64 MPa$\sqrt{m}$. Our tests were performed at $R = 0.1$, which gives $\Delta K = 4$ MPa$\sqrt{m}$ (taking $\Delta K = \Delta K_{\text{eff}}/(1 - R)$. This value corresponds to

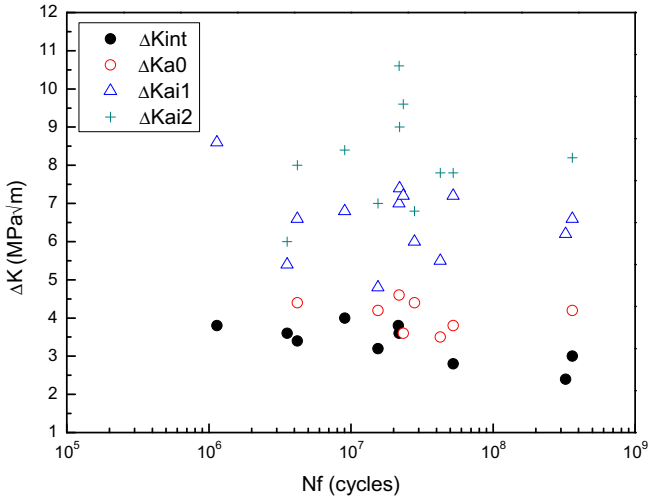

Fig. 25. Evolution of ΔK_{aint}, ΔK_{a_0}, ΔK_{ai1} and ΔK_{ai2} with number of cycles (for the bearing steel).

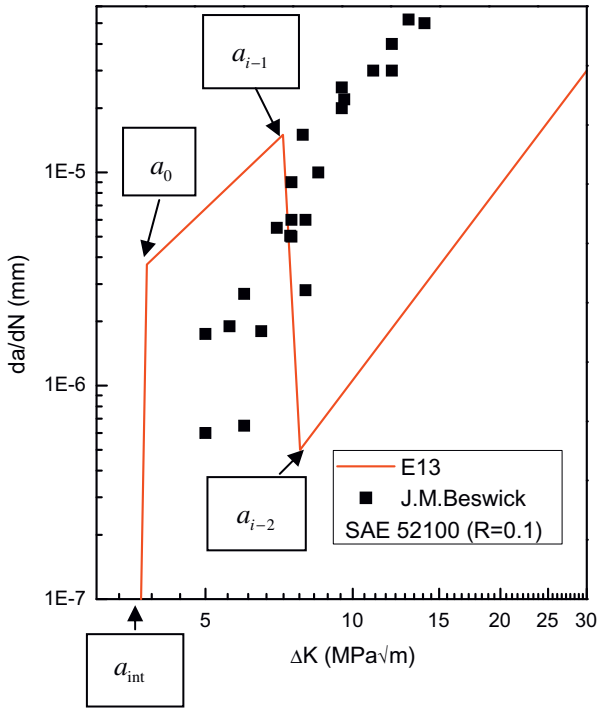

Fig. 26. Comparison of the measured (from Sakai [3]) and calculated growth rates for the mechanical model for specimen E13 (bearing steel).

ΔK_{a_0} and is in very excellent agreement with the mean value (4 MPa$\sqrt{m}$)) given in the Fig. 25.

The transition short crack to long crack is obtained for a mean stress intensity factor $\Delta K_{a_{i1}}$ equal to 6.6 MPa$\sqrt{m}$ (Fig. 25). The difference between $\Delta K_{a_{i1}}$ and ΔK_{a_0} (factor x in the mechanical model) was about 2.6 MPa$\sqrt{m}$. This factor x was observed [6] at a maximum of around three for low load ratios ($R = 0$), and is in very good agreement with the mean experimental value obtained on the low-alloyed steels.

For specimen E13 (see Table 1), the stress intensity factor ΔK (ΔK_{a_0}, $\Delta K_{a_{i-1}}$ and $\Delta K_{a_{i-2}}$) was calculated ($\Delta K = 2\Delta\sigma/\pi\sqrt{\pi a}$) from the measured cracks on SEM micrographs (a_0, a_{i-1} and a_{i-2}). The threshold was taken as $\mathbf{b} = 0.3$ nm and the slope of crack growth rate as three. Before the threshold (between a_{int} and a_0) the slope was taken to be 100. Factor x (Fig. 2) was equal to 3.4 MPa$\sqrt{m}$ for this specimen, which gives $x^3 = 39.2$ (MPa$\sqrt{m}$)^3 (Fig. 2). These calculations produced in Fig. 26. In Fig 26, the crack propagation rate da/dN vs. ΔK measured for bearing steels (at $R = 0.1$) from Sakai [3] is reported (black squares), which agrees very well with the results of this study.

6. Conclusion

The different zones of a fish-eye in the gigacycle fatigue domain have been imaged using OM and SEM. The fractographic results show zones in agreement with the mechanical model.

- A dark area zone (a_{int} to a_0) due to the formation of irreversible persistent slip bands.
- A penny-shaped zone (a_0 to a_{i-1}, crack growth stage I). Whatever the crack initiation site (spherical or elongated inclusion, supergrain or pore), the fracture surface became circular (penny-shaped) around the initiation site.
- A zone with small radial ridges (a_{i-1} to a_{i-2}) corresponding to the short to long crack transition centered on a_i.
- A zone with large radial ridges (a_i to a, crack growth stage II). In this zone fatigue crack propagation produces striations for which the mean distance between striations is a function of ΔK^2, in good agreement with the CTOD.

For the bearing steels studied, whatever the number of cycles at failure N_f, ΔK_{aint}, ΔK_{a_0}, $\Delta K_{a_{i-1}}$ and $\Delta K_{a_{i-2}}$ remained constant or decreased slightly, which is expected for the same material.

References

[1] Bathias C, Paris PC. Gigacycle fatigue in mechanical practice. New York: Marcel Dekker; 2005.

[2] Murakami Y. The mechanism of fatigue failure of steels in the ultralong life regime of $N > 10^7$ cycles. In: Metal fatigue effects of small defects and non-metallic inclusions. Oxford, UK: Elsevier; 2002.

[3] Sakai T. Review and prospects for current studies on very high cycle fatigue of metallic materials for machine structural use. In: Allison JE, Jones JW, Larsen JM, Ritchie RO, editors. Proceedings very high cycle fatigue 4. Warrendale, PA: The Minerals, Metals and Materials Society; 2007.

[4] Shiozawa K, Morii Y, Nishino S, Lu L. Int J Fatigue 2006;28: 1521–32.

[5] Mughrabi H. Int J Fatigue 2006;28:1501–8.

[6] Paris PC, Marines-Garcia I, Hertzberg RW. The relationship of effective stress intensity, elastic modulus and Burgers-vector on fatigue crack growth as associated with "fish eye" ≫ gigacycle phenomena. In: Proceedings of very high cycle fatigue 3. Warrendale, PA: The Minerals, Metals and Materials Society; 2004.

[7] Marines-Garcia I, Paris PC, Tada H, Bathias C. Int J Fatigue 2007;29:2072–8.

[8] Wagner D, Ranc N, Bathias C. Study of fatigue crack growth in gigacycle fatigue domain by thermal analysis during the tests. In: Allison JE, Jones JW, Larsen JM, Ritchie RO, editors. Proceedings of very high cycle fatigue 4. Warrendale, PA: The Minerals, Metals and Materials Society; 2007.

[9] Ranc N, Wagner D, Paris P. Acta Mater 2008;56:4012–21.

[10] Wagner D, Ranc N, Bathias C, Paris P. Fatigue Fract Eng Mater Struct 2009;33:12–21.

[11] Takai K, Honma Y, Izutsu K, Nagumo MJ. Jpn Inst Met 1996; 60(12):1155–62.

[12] Petit J, Sarrazin-Baudoux C. Effet de l'environnement. In: Bathias C, Pineau A, editors. Fatigue des Matériaux et des structures 2. Paris: Lavoisier; 2008.